Journal of Materials Chemistry C

PAPER

View Article Online
View Journal | View Issue

Cite this: J. Mater. Chem. C, 2015, 3, 9292

Structural distortions of the spin-crossover material $[Co(pyterpy)_2](TCNQ)_2$ mediated by supramolecular interactions†

Xuan Zhang,[a] Haomiao Xie,[a] Maria Ballesteros-Rivas,[a] Zhao-Xi Wang[b] and Kim R. Dunbar*[a]

Received 22nd June 2015,
Accepted 2nd August 2015

DOI: 10.1039/c5tc01851j

www.rsc.org/MaterialsC

The incorporation of $TCNQ^{\bullet -}$ (7,7,8,8-tetracyanoquinodimethane) radicals as counterions for the spin-crossover material $[Co(pyterpy)_2](TCNQ)_2$·solvent (pyterpy = 4′-(4′′′-pyridyl)-2,2′:6′,2″-terpyridine) leads to structural distortions of the $[Co(pyterpy)_2]^{2+}$ spin-crossover cation as compared to $[Co(pyterpy)_2](PF_6)_2$. Variable temperature structural and magnetic studies indicate that the supramolecular π-stacking interactions between the terminal pyridyl groups and TCNQ radicals play a crucial role in the spin-crossover properties.

Introduction

Spin-crossover (SCO) is a phenomenon that occurs when the spin state of a complex can be switched between a high spin and low spin state with changes in temperature or upon application of external stimuli such as light and pressure. Such magnetic bistability renders them candidates for applications as sensors as well as memory and display devices.[1] The most common spin-crossover (SCO) materials are octahedral Fe(II) compounds in which the spin transition involves a change in electronic structure from $t_{2g}^6eg^0 \leftrightarrow t_{2g}^4e_g^{2}$.[2] The spin transitions can be abrupt and exhibit hysteresis if strong cooperative interactions between the spin centers are present.[3]

In stark contrast to the plethora of known Fe(II) SCO species, Co(II)-based SCO materials are more scarce and their spin state transformation is generally more gradual because only one electron is involved in the spin-transition in an octahedral geometry, *viz.*, from $t_{2g}^6eg^1 \leftrightarrow t_{2g}^5e_g^{2}$.[4] Among the most widely studied Co(II)-based SCO materials are salts of $[Co(terpy)_2]^{2+}$ (terpy = 2,2′;6′,2″-terpyridine) for which it is known that counterion identity and the presence of interstitial solvent both affect the magnetic properties.[5] For example, $[Co(terpy)_2](ClO_4)_2$ and $[Co(terpy)_2](BF_4)_2$ exhibit SCO behavior but $[Co(terpy)_2](PF_6)_2$ does not; instead, the latter exists in a HS ground state with a small fraction of LS states being populated even at room temperature.[6] The 4′-substituted terpy derivatives with hydroxyl, alkyl, alkoxyl groups have also been extensively investigated and it was found that the presence of long alkyl chains promote interesting properties and/or phase such as reverse spin-transition, re-entrant spin-transition, liquid crystalline SCO materials and SCO films.[7]

One of the main challenges in SCO research is the initiation of cooperative interactions between the individual spin centers, the presence of which induces sharp spin transitions and a memory effect as evidenced by thermal hysteresis.[8] A leading strategy to this end is to incorporate SCO entities into coordination polymers with chemical linkages that assist in enhancing cooperative interactions.[9] Another approach is to take advantage of supramolecular interactions such as hydrogen bonding, π-stacking between the aromatic fragments and interdigitation of long alkyl chains attached to discrete SCO units.[7c,10] In this study, we employ Co(II)-based SCO complexes with an expanded aromatic system with the aim of studying the effects of inter-molecular π-stacking of the planar terpy ligands and TCNQ radicals on the magnetic properties of the resulting materials. In addition, we reasoned that, as TCNQ radical stacks are well known for their electrical conducting properties, inter-molecular interactions between the SCO moieties and TCNQ radicals could lead to bifunctional SCO conductors.[11] Of relevance to the present study is the previously demonstrated work from our group and others that organocyanide radicals such as $TCNQ^{\bullet -}$ (7,7,8,8-tetracyanoquinodimethane) effectively enhance properties through supramolecular π-stacking interactions.[12]

Herein we report the syntheses and variable temperature structural, magnetic and electrical conducting properties of the bifunctional SCO conducting material, $[Co(pyterpy)_2](TCNQ)_2$·DMF·MeOH (**2a**) (pyterpy = 4′-(4′′′-pyridyl)-2,2′:6′,2″-terpyridine). The related solvate $[Co(pyterpy)_2](TCNQ)_2$·MeCN·MeOH (**2b**) was also isolated and investigated in order to probe the effect of solvent molecules on the SCO properties. The compound

[a] Department of Chemistry, Texas A&M University, College Station, TX 77842-3012, USA. E-mail: dunbar@chem.tamu.edu
[b] Department of Chemistry, College of Science, Shanghai University, Shanghai 200444, China

† Electronic supplementary information (ESI) available. CCDC 1403742–1403750. For ESI and crystallographic data in CIF or other electronic format see DOI: 10.1039/c5tc01851j

$[Co(pyterpy)_2](PF_6)_2$ (**1**) was used as a control in this study for documenting the structural distortions and inter-molecular interactions observed in the TCNQ radical SCO materials. It was found that supramolecular π-stacking interactions exist between $TCNQ^{\bullet -}$ radicals and the aromatic pyridyl fragments of the $[Co(pyterpy)_2]^{2+}$ cations which affect the SCO events.

Results and discussion

Variable temperature single crystal X-ray studies

$[Co(pyterpy)_2](PF_6)_2$ (1). Variable temperature single-crystal X-ray crystallography is a powerful tool for the investigation of structure–property relationships in SCO materials due to the fact that the metal–ligand bond distances in these "breathing" materials go through distinct changes with thermal perturbation.[13]

Single crystal X-ray diffraction studies reveal that **1** crystallizes in the tetragonal space group $I4_1/a$ with an asymmetric unit composed of one-quarter of a $[Co(pyterpy)_2]^{2+}$ cation and one-half of a $[PF_6]^-$ anion (Fig. 1). Variable temperature single crystal X-ray studies reveal that the space group remains the same at the temperatures 110, 150, 180 and 300 K (Table S1, ESI†). At 110 K, the Co(II) ion is in a compressed octahedral environment with short axial Co–N1 bond distances of 1.923(5) Å, elongated equatorial Co–(N2) distances of 2.101(3) Å and N1–Co1–N2 bond angles of 78.9(1)°. The Co1–N1 and Co1–N2 bond distances and unit cell parameters exhibit a uniform decrease from 300 to 150 K, below which temperature they display an unusual increase at 110 K (Fig. 2 and Fig. S1, ESI†) which is the result of a Jahn–Teller distortion of the ^2E state of LS Co(II) centers as observed before by Halcrow and coworkers in $[Co(terpy)_2](BF_4)_2$ below 100 K.[6b] The typical structural breathing behavior is that one breathing cycle of contraction and expansion of the metal coordination sphere with temperature occurs during a full cooling and warming cycle.[13b] In contrast, the structural changes in compound **1** exhibits an unusual "double breathing" phenomenon in which two cycles of contractions and expansions of the Co(II) coordination sphere are completed as the temperature goes in one full cooling and warming cycle in the range of 110–300 K.

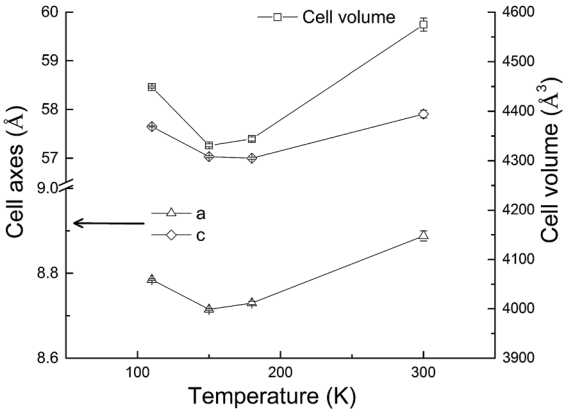

Fig. 2 Temperature dependence of the unit cell parameters of **1** with the estimated standard deviation included.

The terminal pyridyl group (Py(N3)) engages in π-stacking interactions between individual molecules along two directions (*a* and *b* axes) accompanied by the rotation of Py(N3) by 35.46° from the main terpy plane (Fig. 3). The peripheral (Py(N2)) pyridyl rings stack with only a single nearest neighbor with no long-range stacking interactions.

$[Co(pyterpy)_2](TCNQ)_2$ solvates. Metathesis reactions of $[Co(pyterpy)_2](PF_6)_2{\cdot}H_2O$ and LiTCNQ in mixtures of methanol and DMF or methanol and acetonitrile lead to dark purple crystalline products of $[Co(pyterpy)_2](TCNQ)_2{\cdot}DMF{\cdot}MeOH$ (**2a**) or $[Co(pyterpy)_2](TCNQ)_2{\cdot}MeCN{\cdot}MeOH$ (**2b**), respectively. The two products crystallize in the same space group with similar unit cell parameters and packing patterns, the only difference being the presence of interstitial DMF or acetonitrile molecules. Consequently, variable temperature X-ray diffraction studies were conducted only on a crystal of **2a** whose space group and packing patterns remain the same at 110, 150, 180 and 300 K. The compound crystallizes in the triclinic $P\bar{1}$ space group with a cationic $[Co(pyterpy)_2]^{2+}$ unit, two $TCNQ^{\bullet -}$ radicals, one DMF and one methanol molecule in the asymmetric unit (Fig. 4). The crystals gradually lose methanol as evidenced by the single crystal X-ray diffraction data at 300 K where the methanol molecule is best refined with a partial occupancy (Table 1). The same single crystal was used for all the variable temperature

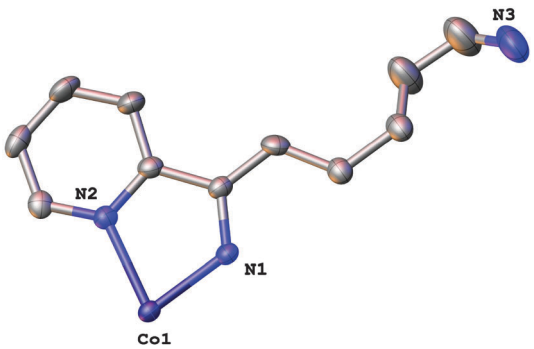

Fig. 1 Asymmetric unit of the crystal structure of **1** with thermal ellipsoids drawn at the 50% probability level. The disordered $[PF_6]^-$ anions and the hydrogen atoms are omitted for the sake of clarity.

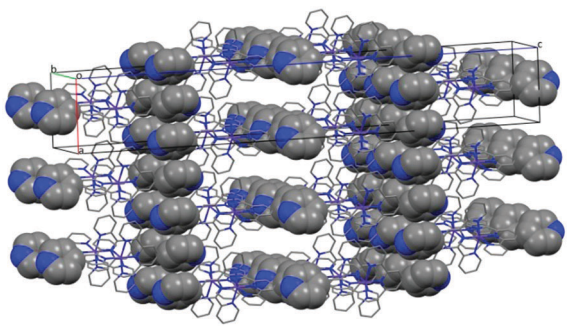

Fig. 3 Packing diagram of **1** with the stacking interactions of the terminal Py(N3) rings highlighted in the space-filling model. Hydrogen atoms and disordered $[PF_6]^-$ anions are omitted for the sake of clarity.

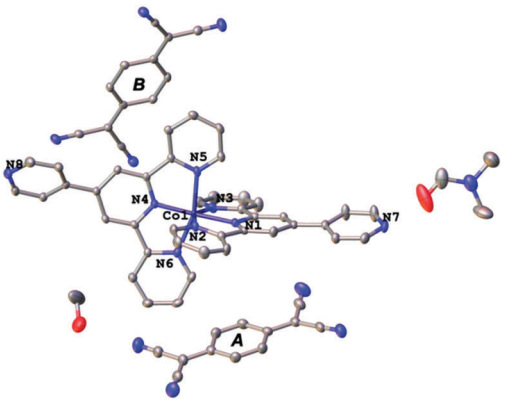

Fig. 4 Asymmetric unit in the crystal structure of **2a** with thermal ellipsoids drawn at the 50% probability level. The hydrogen atoms are omitted for the sake of clarity.

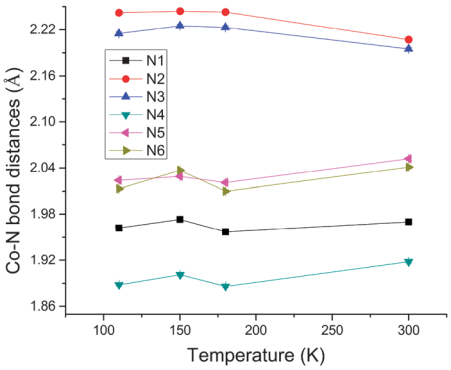

Fig. 5 Temperature dependence of the Co–N bond distances of **2a**.

X-ray diffraction studies. One of the TCNQ radical anions is engaged in hydrogen bonding with a methanol molecule with a N···O distance of 2.903(4) Å (110 K). The Co(II) ion is in a similar compressed octahedral geometry but is distorted in such a fashion that the metal ion is closer to the N4 in the pyterpy ligands along the N4–Co1–N1 direction as compared to the situation for **1** as evidenced by the Co–N bond distances (**2a** at 110 K, Co1–N1 = 1.962(2) Å, Co1–N2 =2.242(2) Å, Co1–N3 = 2.215(2) Å, Co1–N4 = 1.888(2) Å, Co1–N5 = 2.024(2) Å, Co1–N6 = 2.013(2) Å, Table S2, ESI†). The two equatorial Co–N2 and Co–N3 bonds are quite elongated and thermal effects have a relatively small influence on them. The other four Co–N bond distances decrease as the temperature is lowered from 300 to 180 K and then experience an unusual increase from 180 to 150 K which is presumably due to a Jahn–Teller distortion of the ^{2}E state of LS Co(II) as found for **1** (Fig. 5). The difference in this case is that the unusual elongation is observed below 180 K for **2a** as opposed to 150 K in **1**. The higher temperature for the elongation in **2a** indicates that the lower local symmetry of the Co(II) center helps to stabilize the LS state more than does the higher local symmetry present in **1**. A "double breathing" behavior is also reflected in the unit cell *b* and *c* dimensions and the contraction in the volume from 300 to 180 K and then expansion from 180 to 150 K (Fig. S8, ESI†).

Table 1 Pertinent crystallographic data for **2a** at different temperatures

	110 K	150 K	180 K	300 K
Empirical formula	$C_{68}H_{47}CoN_{17}O_2$	$C_{68}H_{47}CoN_{17}O_2$	$C_{68}H_{47}CoN_{17}O_2$	$C_{67.61}H_{43}CoN_{17}O_{1.25}$
Formula weight	1193.15	1193.15	1193.15	1172.44
Temperature/K	110	150	180	300
Crystal system	Triclinic	Triclinic	Triclinic	Triclinic
Space group	$P\bar{1}$	$P\bar{1}$	$P\bar{1}$	$P\bar{1}$
a/Å	8.911(5)	8.941(7)	8.981(3)	8.986(4)
b/Å	13.921(8)	13.990(11)	13.924(4)	13.909(6)
c/Å	24.708(15)	24.828(19)	24.722(8)	24.825(11)
α/°	74.249(7)	74.116(9)	74.006(11)	105.759(6)
β/°	81.736(8)	82.082(10)	81.940(11)	95.448(6)
γ/°	85.755(7)	85.910(10)	85.735(12)	94.088(6)
Volume/Å^3	2917(3)	2957(4)	2940.4(16)	2957(2)
Z	2	2	2	2
ρ_{calc}/g cm^{-3}	1.358	1.340	1.348	1.317
μ/mm^{-1}	0.358	0.353	0.355	0.351
F(000)	1234.0	1234.0	1234.0	1209.0
Crystal size/mm^3	0.25 × 0.13 × 0.08	0.25 × 0.13 × 0.08	0.25 × 0.13 × 0.08	0.25 × 0.13 × 0.08
Radiation	MoKα (λ = 0.71073)	MoKα (λ = 0.71073)	MoKα (λ = 0.71073)	MoKα (λ = 0.71073)
2Θ range for data collection/°	3.042 to 52.044	3.028 to 53.464	3.07 to 52.044	3.058 to 53.466
Index ranges	$-10 \le h \le 10$, $-17 \le k \le 17$, $-30 \le l \le 30$	$-11 \le h \le 11$, $-17 \le k \le 17$, $-31 \le l \le 31$	$-11 \le h \le 11$, $-17 \le k \le 16$, $-30 \le l \le 30$	$-11 \le h \le 11$, $-17 \le k \le 17$, $-31 \le l \le 31$
Reflections collected	30 512	31 031	25 859	33 075
Independent reflections	11 425 [R_{int} = 0.0983, R_{sigma} = 0.0935]	12 363 [R_{int} = 0.0428, R_{sigma} = 0.0538]	11 436 [R_{int} = 0.0718, R_{sigma} = 0.0736]	12 505 [R_{int} = 0.0424, R_{sigma} = 0.0584]
Data/restraints/parameters	11 425/0/797	12 363/0/797	11 436/0/797	12 505/0/797
Goodness-of-fit on F^2	1.058	1.091	1.049	1.024
Final *R* indexes [$I \ge 2\sigma(I)$]	R_1 = 0.0508, wR_2 = 0.1228	R_1 = 0.0461, wR_2 = 0.1388	R_1 = 0.0446, wR_2 = 0.1187	R_1 = 0.0475, wR_2 = 0.1011
Final *R* indexes [all data]	R_1 = 0.0759, wR_2 = 0.1379	R_1 = 0.0607, wR_2 = 0.1560	R_1 = 0.0580, wR_2 = 0.1287	R_1 = 0.0871, wR_2 = 0.1195
Largest diff. peak/hole/e Å^{-3}	0.99/−0.68	0.67/−0.66	0.64/−0.48	0.20/−0.30

$R_1 = \Sigma||F_o| - |F_c||/\Sigma|F_o|$. w$R_2 = [\Sigma w(|F_o| - |F_c|)^2/\Sigma w(F_o)^2]^{1/2}$. w = $0.75/(\sigma^2(F_o) + 0.00010F_o^2)$.

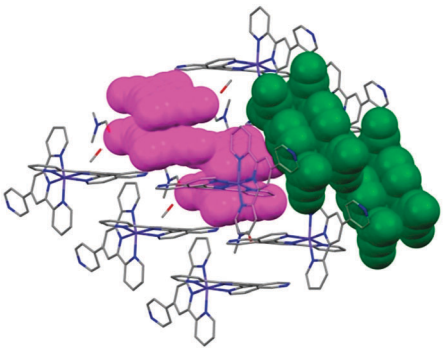

Fig. 6 Packing view of the crystal structure of **2a** highlighting the stacking interactions between the TCNQ dimers of AA (magenta) and BB (green) in the space-filling model.

The additional terminal pyridyl groups in **2a** are involved in π-stacking interactions with TCNQ radicals to varying degrees owing to the different rotational orientations present. The rotations of Py(N7) to Py(N1) and Py(N8) to Py(N4) are approximately 13.78 and 36.51°, respectively. Due to the relatively sizeable rotation of the Py(N8) ring, it can only stack with the Py(N8) ring of another $[Co(pyterpy)_2]^{2+}$ cation whereas the less rotated Py(N7) ring is engaged in inter-molecular stacking with closer contacts of both the Py(N1) and Py(N7) rings (Fig. S4, ESI†). In addition to these rotations, the structural distortion of **2a** as compared to **1** is reflected in the bending of the pyridyl rings (Fig. 4).

As depicted in Fig. 6, the two unique TCNQ radicals in the asymmetric unit designated as A and B are stacked as AA and BB dimers with inter-planar distances of ~3.217 and 3.088 Å, respectively (Fig. 6). Furthermore, the TCNQ dimers AA engage in interactions with two stacked Py(8) rings of the $[Co(pyterpy)_2]^{2+}$ cations in an alternating AA–Py(8)Py(8)–AA fashion (Fig. 7). As for the TCNQ dimers BB, these are separated by the $[Co(pyterpy)_2]^{2+}$ cations (Fig. S5, ESI†) with no additional contacts. In contrast to **1**, in which only the pyridyl groups of the $[Co(pyterpy)_2]^{2+}$ cations are available for stacking, the π-interactions between the pyridyl groups and TCNQ radical anions in **2a** provide secondary ligand sphere modulation effects on the $[Co(pyterpy)_2]^{2+}$ SCO units.

Magnetic properties

Inorganic salts of $[Co(pyterpy)_2]^{2+}$ are known and have been investigated for their biological activities, but no magnetic properties for these compounds have been reported.[14] Magnetic measurements

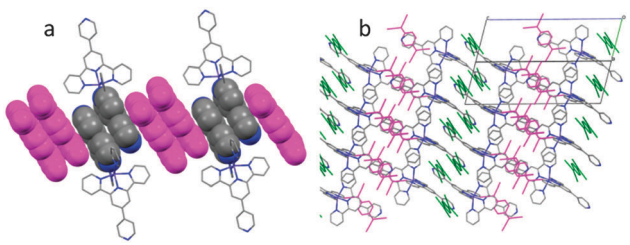

Fig. 7 Side view (a) and top view (b) in the crystal structure of **2a** highlighting the stacking interactions between the TCNQ dimers of AA (magenta) and the Py(8)Py(8) stacked dimers.

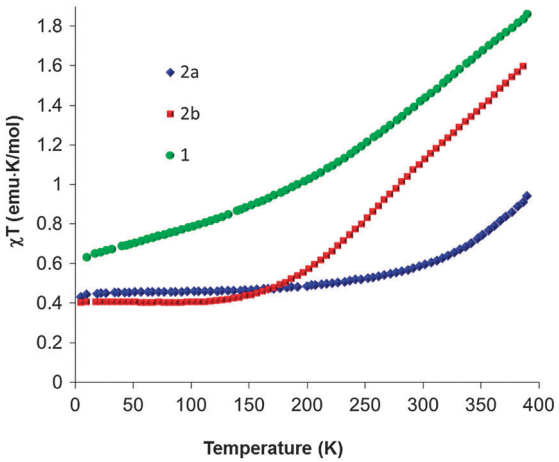

Fig. 8 Temperature dependence of $\chi_M T$ *versus* T plots for compounds **1**, **2a** and **2b**.

were carried out on freshly prepared crystalline powders of **1**, **2a** and **2b** in gel capsules from T = 5–390 K at a cooling/heating rate of 5 K min^{-1}. The phase purities of the freshly prepared bulk crystalline powders were verified by powder X-ray diffraction studies (Fig. S6 and S7, ESI†). Compound **1**, measured as a control experiment for the non-innocent TCNQ radical anion salts, exhibits a very gradual spin transition that does not reach a fully populated LS state even at 5 K with a $\chi_M T$ value of 0.61(1) emu K mol^{-1} (Fig. 8). At room temperature, the $\chi_M T$ value of 1.42(1) emu K mol^{-1} corresponds to ~56% of Co(II) in the HS state (g = 2.16).‡ Similar behavior was recently reported by Brooker and coworkers for a closely related compound $[Co(py\text{-}pzpypz)_2](BF_4)_2$ (py-pzpypz = (4-(4-pyridyl)-2,5-dipyrazyl-pyridine)).[15]

Compounds **2a** and **2b** exhibit typical Co(II) gradual spin-crossover with LS $\chi_M T$ values of 0.45 emu K mol^{-1} and 0.41 emu K mol^{-1}, respectively. These values are higher than the spin-only values for LS Co(II), which is attributed to spin–orbit coupling. At 300 K, **2a** and **2b** show $\chi_M T$ values of 0.58 and 1.11 emu K mol^{-1}, corresponding to ~7% and 39% HS population of Co(II) (g = 2.19), respectively.‡ At 390 K, **2a** and **2b** exhibit $\chi_M T$ values of 0.94 and 1.63 emu K mol^{-1}, corresponding to ~27% and 67% HS population of Co(II), respectively. The $T_{1/2}$ value (the temperature at which the SCO molecules are equally populated in the HS/LS state) of compound **2b** is ~332 K, whereas the value for **2a** is clearly higher than 390 K but cannot be determined from the experimental data due to instrument limit. Below ~180 K, the Co(II) ions in compound **2a** are almost entirely in the LS state. The LS states of Co(II) in **2b**, however, are not fully populated until below 110 K. The spins on the TCNQ radicals are paired due to the close contacts of the TCNQ radical dimers in the structure of **2a** and **2b**, therefore they would not be expected to contribute to the magnetic moment.[12a] The cooling and warming curves of the χT plots of all three compounds exhibit no discernible hysteresis, which is common for similar Co(II) SCO systems.[15,16]

As the structural analyses indicate, the cell parameters for crystals of **1** exhibit only one important change at ~150 K as

‡ The g value was obtained from the χT magnitude of the LS Co(II) state.

the temperature decreases with no discernible changes down to 110 K (Fig. 2). In contrast, the trend in the changes of the *b* and *c* unit cell edges and the unit cell volume for **2a** exhibit two anomalies at ~180 and 150 K, namely a decrease in values from ~300–180 K, an increase in the range ~180–150 K, and then a second decrease below 150 K (Fig. S8, ESI†). These results indicate that the Jahn–Teller distortion in the high symmetry ($I4_1/a$) compound **1** occurs at lower temperatures as compared to **2a** with a lower symmetry which results in an incomplete transition from HS to LS in the former compound at 110 K, but a nearly complete transition to LS for **2a** below 180 K.

The effect of solvent molecules also plays an important role in the spin-transition of $[Co(pyterpy)_2](TCNQ)_2$·solvent compounds. As mentioned earlier, compounds **2a** and **2b** crystallize in the same space group and exhibit similar packing patterns, with the only difference being the presence of DMF *versus* acetonitrile solvent molecules. It has been reported for 3-D Fe(II) SCO frameworks that smaller solvent molecules tend to exert a higher chemical pressure and stabilize the LS state.[17] In our case, however, the higher $T_{1/2}$ of **2a** as compared to **2b** is attributed to a higher overall chemical pressure induced by the larger DMF molecules which help to stabilize the LS states more than the smaller acetonitrile molecules in **2b**. This cannot be simply rationalized by the size of the solvent molecule because, besides the difference in SCO systems (Fe(II) *vs.* Co(II)), in discrete molecular complexes the positions of SCO entities can shift to mitigate the effect of size variation in the interstitial solvents. In addition, the shape, orientation and the electronic effects of the solvent molecules may also play a role.[18]

Conductivity properties

Electrical conductivity studies performed on single crystal samples of **2a** revealed a room temperature conductivity of $\sim 5 \times 10^{-6}$ S cm^{-1}. It is interesting to note that the conductivity, unlike semiconducting materials with TCNQ radicals stacks, is nearly independent of temperature between 300 and 100 K (Fig. S9, ESI†), which is possibly due to a compensation effect of decreased charge-carrier concentration and increased charge carrier mobility as the temperature decreases.[19]

Conclusions

The bifunctional SCO materials $[Co(pyterpy)_2](TCNQ)_2$·solvent with different crystallizing solvents have been synthesized and characterized by variable temperature single crystal X-ray diffraction and magnetic measurements. Strong intermolecular interactions between the SCO centers have been realized by taking advantage of the supramolecular π-stacking interactions between the terminal pyridyl groups of the pyterpy ligands and TCNQ radicals. In comparison to the high symmetry compound **1**, in which the HS to LS transition is incomplete even at 5 K, the radical-pyridyl π-stacking interaction distorts the Co(II) coordination geometry and helps to stabilize the LS ^{2}E state. The design of multifunctional SCO materials with improved cooperativity may benefit from this new strategy of employing organic radicals to enhance intermolecular interactions.

Experimental

Syntheses

The starting materials LiTCNQ, $(Et_3NH)(TCNQ)_2$ and pyterpy were prepared according to literature procedures.[20] The starting material $[Co(pyterpy)_2](ClO_4)_2$ was prepared by a modified procedure from the literature.[14] **Caution!** Perchlorates are potentially explosive and should be handled very carefully in small amounts. Avoid heat, drying and grinding.

$[Co(pyterpy)_2](ClO_4)_2$. $Co(ClO_4)_2·6H_2O$ (0.6 mmol, 0.220 g) was dissolved in 9 mL of MeCN : H_2O (v : v = 1 : 2) solvent. A suspension of pyterpy (1.2 mmol, 0.352 g) in 5 mL of MeCN was slowly added to the solution to yield a dark red suspension. After stirring for 2 hours at room temperature, 5 mL H_2O was added. The reaction mixture was concentrated to ~10 mL by evaporation in air. The precipitate was collected by filtration, washed with water and dried in air to obtain 0.40 g (76% yield) of red powder.

$[Co(pyterpy)_2](PF_6)_2·H_2O$. A suspension of pyterpy (1 mmol, 0.310 g) in 5 mL of MeCN : MeOH (v : v = 4 : 1) was added into a solution of $Co(OAc)_2·4H_2O$ (0.5 mmol, 0.125 g) in 5 mL of methanol. The color of the solution turned dark red, and after stirring for 2 hours, 10 mL of an aqueous solution of KPF_6 (1.5 mmol, 0.277 g) was added and the mixture was stirred for another hour. The precipitate was filtered, washed with water and dried in air to afford 0.39 g (79% yield) of red-orange product. Elemental analysis: calculated (%) for $C_{40}H_{28}CoN_8P_2F_{12}·H_2O$: C(48.65), H(3.06), N(11.35); found: C(48.83), H(2.99), N(11.36).

$[Co(pyterpy)_2](PF_6)_2$ (1). Red crystals of solvent free $[Co(pyterpy)_2](PF_6)_2$ were obtained by diffusing diethyl ether vapor into a DMF solution of $[Co(pyterpy)_2](PF_6)_2·H_2O$. The phase purity of the freshly prepared bulk crystalline powder was verified by powder X-ray diffraction. See Table S1 (ESI†) for single crystal X-ray crystallography data.

$[Co(pyterpy)_2](TCNQ)_2$·DMF·MeOH (2a). $[Co(pyterpy)_2](PF_6)_2·H_2O$ (0.1 mmol, 97 mg) in 2 mL of DMF : MeOH (v : v = 1 : 1) was layered with LiTCNQ (0.20 mmol, 42.2 mg) in 4 mL of MeOH in a 3 dram vial. After the solution had been left undisturbed for 30 minutes, 71 mg of dark purple crystals were collected by filtration (34% yield). The phase purity of the freshly prepared bulk crystalline powder was verified by powder X-ray diffraction. See Table 1 for variable temperature single crystal X-ray crystallography data. After standing in air, the fresh sample tended to partially lose methanol and pick up water. Elemental analysis: calculated (%) for $C_{64}H_{36}CoN_{16}·0.75CH_3OH·DMF·1.85H_2O$: C(66.78), H(4.11), N(19.54); found: C(66.61), H(3.97), N(19.71). IR: Nujol mulls on KBr plates: ν(OH) 3369.7 cm^{-1}, ν(CN) 2196.1, 2178.6 and 2165.9 cm^{-1}, δ(C–H, TCNQ) 822.9 cm^{-1}.

$[Co(pyterpy)_2](TCNQ)_2$·MeCN·MeOH (2b). A sample of $[Co(pyterpy)_2](ClO_4)_2$ (0.10 mmol, 87.7 mg) was dissolved in 10 mL of a MeCN : MeOH (v : v = 4 : 1) mixture, filtered and

then slowly treated with a solution of $(Et_3NH)(TCNQ)_2$ (0.10 mmol, 50 mg) in 5 mL acetonitrile. After standing for 30 minutes, the reaction mixture was filtered to obtain 40 mg of dark purple crystals (61% yield). IR: Nujol mulls on KBr plates: ν(OH) 3372.4 cm^{-1}, ν(CN) 2195.1, 2178.6 and 2165.9 cm^{-1}, δ(C–H, TCNQ) 822.9 cm^{-1}. The phase purity of the freshly prepared bulk crystalline powder was verified by powder X-ray diffraction. Crystal data for $C_{67}H_{43}CoN_{17}O$ (M =1161.11 g mol^{-1}): triclinic, space group $P\bar{1}$ (no. 2), a = 8.939(3) Å, b = 13.632(5) Å, c = 24.204(8) Å, α = 76.313(4)°, β = 81.950(4)°, γ = 87.007(4)°, V = 2836.8(16) $Å^3$, Z = 2, T = 110 K, μ(MoKα) = 0.365 mm^{-1}, D_{calc} = 1.359 g cm^{-3}, 26 219 reflections measured ($3.076° \leq 2\Theta \leq 48.81°$), 9330 unique ($R_{int}$ = 0.1068, R_{sigma} = 0.0951) which were used in all calculations. The final R_1 was 0.0502 ($I > 2\sigma(I)$) and wR_2 was 0.1254 (all data).

Magnetic and conductivity measurements

Magnetic measurements over the temperature range of 5–390 K were carried out using a Quantum design MPMS-XL SQUID magnetometer. The diamagnetic contributions of the compounds and sample holders were accounted for during the data analysis process by using Pascal's constants. Single crystal conductivity measurements were performed by the two-probe method on the MPMS-XL SQUID magnetometer over the temperature range of 100–300 K with a constant current source.

Single crystal X-ray crystallography

Single-crystal X-ray data were collected at different temperatures on a Bruker APEX CCD diffractometer equipped with a graphite monochromated MoKα radiation source (λ = 0.71073 Å). Suitable crystals were affixed onto a nylon loop with paratone oil and place in a cold steam of N_2(g). The data sets were recorded by the ω-scan method and integrated followed by an absorption correction in the Bruker APEX II software package. Solution and refinement of the crystal structures were carried out using the SHELXT[21] and SHELXL[22] programs and the graphical interface Olex2.[23] Hydrogen atoms were placed at calculated positions. A summary of pertinent information relating to unit cell parameters are provided in Table 1 and Table S1 (ESI†). CCDC 1403742–1403750.

Acknowledgements

This material is based on work supported by the US Department of Energy, Materials Sciences Division, under Grant No. DE-SC0012582. Dr Z.-X. Wang thanks the China Scholarship Counsel (No. 201206895004) and National Natural Science Foundation of China (No. 21171115) for financial support. MFBR thanks Secretaria de Ciencia y Tecnologia del Distrito Federal (SECITI).

Notes and references

1 (*a*) B. Weber, *Spin-Crossover Materials*, John Wiley & Sons Ltd, 2013, ch. 2, pp. 55–76, DOI: 10.1002/9781118519301; (*b*) F. Prins, M. Monrabal-Capilla, E. A. Osorio, E. Coronado and H. S. J. van der Zant, *Adv. Mater.*, 2011, **23**, 1545–1549; (*c*) J.-F. Létard, P. Guionneau and L. Goux-Capes, *Spin Crossover in Transition Metal Compounds III*, Springer, Berlin Heidelberg, 2004, vol. 235, ch. 10, pp. 221–249; (*d*) Y. Garcia, V. Ksenofontov, S. Mentior, M. M. Dîrtu, C. Gieck, A. Bhatthacharjee and P. Gütlich, *Chem. – Eur. J.*, 2008, **14**, 3745–3758.

2 (*a*) M. A. Halcrow, *Coord. Chem. Rev.*, 2009, **253**, 2493–2514; (*b*) A. Santoro, L. J. Kershaw Cook, R. Kulmaczewski, S. A. Barrett, O. Cespedes and M. A. Halcrow, *Inorg. Chem.*, 2015, **54**, 682–693.

3 (*a*) A. Hauser, J. Jeftić, H. Romstedt, R. Hinek and H. Spiering, *Coord. Chem. Rev.*, 1999, **190–192**, 471–491; (*b*) P. Gütlich, A. B. Gaspar and Y. Garcia, *Beilstein J. Org. Chem.*, 2013, **9**, 342–391.

4 (*a*) I. Krivokapic, M. Zerara, M. L. Daku, A. Vargas, C. Enachescu, C. Ambrus, P. Tregenna-Piggott, N. Amstutz, E. Krausz and A. Hauser, *Coord. Chem. Rev.*, 2007, **251**, 364–378; (*b*) M. G. Cowan, J. Olguín, S. Narayanaswamy, J. L. Tallon and S. Brooker, *J. Am. Chem. Soc.*, 2012, **134**, 2892–2894.

5 (*a*) R. Hogg and R. G. Wilkins, *J. Chem. Soc.*, 1962, 341–350, DOI: 10.1039/JR9620000341; (*b*) S. Kremer, W. Henke and D. Reinen, *Inorg. Chem.*, 1982, **21**, 3013–3022; (*c*) H. Oshio, H. Spiering, V. Ksenofontov, F. Renz and P. Gütlich, *Inorg. Chem.*, 2001, **40**, 1143–1150; (*d*) J. S. Judge and W. A. Baker Jr, *Inorg. Chim. Acta*, 1967, **1**, 68–72.

6 (*a*) C. Enachescu, I. Krivokapic, M. Zerara, J. A. Real, N. Amstutz and A. Hauser, *Inorg. Chim. Acta*, 2007, **360**, 3945–3950; (*b*) C. A. Kilner and M. A. Halcrow, *Dalton Trans.*, 2010, **39**, 9008–9012.

7 (*a*) A. B. Gaspar, M. C. Muñoz, V. Niel and J. A. Real, *Inorg. Chem.*, 2001, **40**, 9–10; (*b*) A. Galet, A. B. Gaspar, M. C. Muñoz and J. A. Real, *Inorg. Chem.*, 2006, **45**, 4413–4422; (*c*) S. Hayami, Y. Shigeyoshi, M. Akita, K. Inoue, K. Kato, K. Osaka, M. Takata, R. Kawajiri, T. Mitani and Y. Maeda, *Angew. Chem., Int. Ed.*, 2005, **44**, 4899–4903; (*d*) P. Nielsen, H. Toftlund, A. D. Bond, J. F. Boas, J. R. Pilbrow, G. R. Hanson, C. Noble, M. J. Riley, S. M. Neville, B. Moubaraki and K. S. Murray, *Inorg. Chem.*, 2009, **48**, 7033–7047; (*e*) S. Hayami, K. Murata, D. Urakami, Y. Kojima, M. Akita and K. Inoue, *Chem. Commun.*, 2008, 6510–6512, DOI: 10.1039/b814415j; (*f*) G. Agusti, C. Bartual, V. Martinez, F. J. Munoz-Lara, A. B. Gaspar, M. C. Munoz and J. A. Real, *New J. Chem.*, 2009, **33**, 1262–1267; (*g*) S. Hayami, *Spin-Crossover Materials*, John Wiley & Sons Ltd, 2013, ch. 12, pp. 321–345, DOI: 10.1002/9781118519301.

8 (*a*) K. Murray and C. Kepert, in *Spin Crossover in Transition Metal Compounds I*, ed. P. Gütlich and H. A. Goodwin, Springer, Berlin Heidelberg, 2004, vol. 233, ch. 8, pp. 195–228; (*b*) J. Olguín and S. Brooker, *Spin-Crossover Materials*, John Wiley & Sons Ltd, 2013, ch. 3, pp. 77–120, DOI: 10.1002/9781118519301; (*c*) M. A. Halcrow, *Chem. Lett.*, 2014, **43**, 1178–1188.

9 (*a*) O. Kahn and C. J. Martinez, *Science*, 1998, **279**, 44–48; (*b*) M. Carmen Muñoz and J. Antonio Real,

Spin-Crossover Materials, John Wiley & Sons Ltd, 2013, ch. 4, pp. 121–146, DOI: 10.1002/9781118519301.

10 (*a*) B. Weber, W. Bauer and J. Obel, *Angew. Chem., Int. Ed.*, 2008, **47**, 10098–10101; (*b*) J.-F. Létard, P. Guionneau, E. Codjovi, O. Lavastre, G. Bravic, D. Chasseau and O. Kahn, *J. Am. Chem. Soc.*, 1997, **119**, 10861–10862; (*c*) S. Hayami, Z.-z. Gu, H. Yoshiki, A. Fujishima and O. Sato, *J. Am. Chem. Soc.*, 2001, **123**, 11644–11650.

11 (*a*) Z. Zhang, H. Zhao, M. M. Matsushita, K. Awaga and K. R. Dunbar, *J. Mater. Chem. C*, 2014, **2**, 399–404; (*b*) X. Zhang, Z. Zhang, H. Zhao, J. G. Mao and K. R. Dunbar, *Chem. Commun.*, 2014, **50**, 1429–1431; (*c*) H. Phan, S. M. Benjamin, E. Steven, J. S. Brooks and M. Shatruk, *Angew. Chem., Int. Ed.*, 2015, **54**, 823–827; (*d*) H. Kubota, Y. Takahashi, J. Harada and T. Inabe, *Cryst. Growth Des.*, 2014, **14**, 5575–5584; (*e*) Z. Zhang, H. Zhao, H. Kojima, T. Mori and K. R. Dunbar, *Chem. – Eur. J.*, 2013, **19**, 3348–3357; (*f*) M. Ballesteros-Rivas, A. Ota, E. Reinheimer, A. Prosvirin, J. Valdes-Martinez and K. R. Dunbar, *Angew. Chem., Int. Ed. Engl.*, 2011, **50**, 9703–9707.

12 (*a*) Z. X. Wang, X. Zhang, Y. Z. Zhang, M. X. Li, H. Zhao, M. Andruh and K. R. Dunbar, *Angew. Chem., Int. Ed.*, 2014, **53**, 11567–11570; (*b*) A. M. Madalan, V. Voronkova, R. Galeev, L. Korobchenko, J. Magull, H. W. Roesky and M. Andruh, *Eur. J. Inorg. Chem.*, 2003, 1995–1999; (*c*) A. M. Madalan, H. W. Roesky, M. Andruh, M. Noltemeyer and N. Stanica, *Chem. Commun.*, 2002, 1638–1639, DOI: 10.1039/B202628G; (*d*) H. Fukunaga and H. Miyasaka, *Angew. Chem., Int. Ed.*, 2015, **54**, 569–573; (*e*) M. A. Dobrowolski, G. Garbarino, M. Mezouar, A. Ciesielski and M. K. Cyranski, *CrystEngComm*, 2014, **16**, 415–429.

13 (*a*) M. A. Halcrow, *Chem. Soc. Rev.*, 2011, **40**, 4119–4142; (*b*) P. Guionneau, *Dalton Trans.*, 2014, **43**, 382–393.

14 R. Indumathy, S. Radhika, M. Kanthimathi, T. Weyhermuller and B. Unni Nair, *J. Inorg. Biochem.*, 2007, **101**, 434–443.

15 R. G. Miller and S. Brooker, *Inorg. Chem.*, 2015, **54**, 5398–5409.

16 L. J. Kershaw Cook, F. Tuna and M. A. Halcrow, *Dalton Trans.*, 2013, **42**, 2254–2265.

17 (*a*) L. Piñeiro-López, Z. Arcís-Castillo, M. C. Muñoz and J. A. Real, *Cryst. Growth Des.*, 2014, **14**, 6311–6319; (*b*) D. Aravena, Z. A. Castillo, M. C. Muñoz, A. B. Gaspar, K. Yoneda, R. Ohtani, A. Mishima, S. Kitagawa, M. Ohba, J. A. Real and E. Ruiz, *Chem. – Eur. J.*, 2014, **20**, 12864–12873.

18 (*a*) P. D. Southon, L. Liu, E. A. Fellows, D. J. Price, G. J. Halder, K. W. Chapman, B. Moubaraki, K. S. Murray, J.-F. Létard and C. J. Kepert, *J. Am. Chem. Soc.*, 2009, **131**, 10998–11009; (*b*) M. Hostettler, K. W. Törnroos, D. Chernyshov, B. Vangdal and H.-B. Bürgi, *Angew. Chem., Int. Ed.*, 2004, **43**, 4589–4594.

19 T. Mishima, T. Ojiro, K. Kajita, Y. Nishio and Y. Iye, *Synth. Met.*, 1995, **70**, 771–774.

20 (*a*) L. R. Melby, R. J. Harder, W. R. Hertler, W. Mahler, R. E. Benson and W. E. Mochel, *J. Am. Chem. Soc.*, 1962, **84**, 3374–3387; (*b*) A. Winter, A. M. J. van den Berg, R. Hoogenboom, G. Kickelbick and U. S. Schubert, *Synthesis*, 2007, 0642.

21 G. Sheldrick, *Acta Crystallogr., Sect. A: Found. Adv.*, 2015, **71**, 3–8.

22 G. Sheldrick, *Acta Crystallogr., Sect. A: Found. Crystallogr.*, 2008, **64**, 112–122.

23 O. V. Dolomanov, L. J. Bourhis, R. J. Gildea, J. A. K. Howard and H. Puschmann, *J. Appl. Crystallogr.*, 2009, **42**, 339–341.

